Calculation of uniaxial magnetic anisotropy energy of tetragonal and trigonal Fe, Co, and Ni

Till Burkert,* Olle Eriksson, Peter James, Sergei I. Simak, Börje Johansson, and Lars Nordström
Department of Physics, Uppsala Universitet, Box 530, 751 21 Uppsala, Sweden
(Received 30 October 2003; published 25 March 2004)

The magnetic anisotropy energy (MAE) of Fe, Co, and Ni is presented for tetragonal and trigonal structures along two paths of structural distortion connecting the bcc and the fcc structure. The MAE was calculated from first principles with the full-potential linear muffin-tin orbital method and the force theorem. As is expected from symmetry considerations, the MAE increases by orders of magnitude when the cubic symmetry is broken. For tetragonal structures of Co and Ni a regular behavior of the MAE is observed, i.e., only the symmetry dictated nodes at the cubic structures appear along this path of distortion. In the case of tetragonal Fe, additional reorientations of the easy axis occur that are attributed to a topological change of the Fermi surface upon distortion. For the trigonal structures of all three elements the strain dependence of the MAE is more complicated, with additional reorientations of the easy axis and an unexpectedly large MAE for certain distortions of Ni, and a strongly nonlinear behavior for trigonal structures of Co close to fcc. Furthermore, the linear magnetoelastic coupling coefficients are calculated from the MAE at small distortions from the cubic equilibrium structure of the three elements. Two different Brillouin-zone integration techniques were used to calculate the MAE. Since the Gaussian broadening method smears out details of the Fermi surface, it results in a different MAE as compared to the tetrahedron method in some cases.

DOI: 10.1103/PhysRevB.69.104426 PACS number(s): 75.30.Gw, 75.70.Ak, 71.20.Be, 75.80.+q

I. INTRODUCTION

Magnetic thin films and multilayers have recently attracted large interest because of their technological importance in data storage and sensor applications as well as in fundamental research of magnetism.[1] Apart from effects that arise at surfaces and interfaces due to the reduced coordination and hybridization with adjacent layers, these artificial heterostructures allow by pseudomorphic growth to stabilize structures that do not exist in bulk. Thin films grown epitaxially on a substrate will adapt its in-plane lattice parameter, if the lattice mismatch is not too large. The lattice parameter perpendicular to the interface will acquire a value that roughly conserves the unit-cell volume of the film. Hence, the cubic symmetry of, e.g., Fe and Ni in bulk will be lowered. To give a few examples, Fe,[2,3] Co,[4] and Ni (Ref. 5)—as well as their alloys[6]—grow epitaxially on Cu(001) with a tetragonally distorted fcc structure. On the other hand, Fe on Ag(001) (Ref. 7) and Ni on Fe(001) and Au(001) (Ref. 8) grow in a body-centered tetragonal (bct) structure. Co can be stabilized in a bct structure by epitaxial growth on GaAs(110) (Ref. 9). Examples for trigonal structures close to fcc are Fe/Cu(111), (Refs. 10 and 11) and Co/Cu(111).[12–14]

A characteristic property of magnetic thin films and multilayers is the enhanced magnetic anisotropy energy (MAE). The MAE for systems with cubic symmetry is very small, of the order of 1 μeV/atom. Layered magnetic materials on the other hand exhibit an uniaxial MAE that is several orders of magnitude larger. Frequently it is observed that the magnetic easy axis is orientated along the film normal. This perpendicular magnetic anisotropy (PMA) is of technological interest in the context of magnetic and magneto-optical data storage media.

The MAE of magnetic materials is usually discussed in terms of several contributions. The so-called shape anisotropy depends on the form of the magnetic specimen. In a magnetic thin film it always favors a magnetization in the film plane. If PMA is observed, the shape anisotropy is overcome by the intrinsic magnetocrystalline anisotropy (MCA). The latter has two distinct contributions, one that arises from the dipole-dipole interaction and another that has its microscopic origin in the relativistic spin-orbit coupling (SOC). In the magnetic transition metals that are studied here, the dipolar contribution to the MCA is much smaller.[15,16] Thus, the main origin of the MAE is the coupling of the spin moment to the crystal lattice via the SOC. In the remainder it is this contribution that will be referred to as MAE. In addition to these volume contributions, the reduced coordination at surfaces and interfaces, as well as the hybridization with adjacent magnetic or nonmagnetic layers, affect the MAE and become increasingly important if the film thickness is reduced.

The origin of the large uniaxial MAE in layered systems can be understood from an expansion of the free-energy density in terms of the magnetization direction relative to the crystal axes.[15] In a cubic crystal only anisotropy constants of fourth and higher order are involved. When the cubic symmetry is broken, second-order anisotropy constants appear due to the splitting of previously degenerate states. Since the magnetic anisotropy constants of order n are proportional to $(\xi/W)^n$,[15] where ξ is the strength of the SOC and W is the width of the d band, a lowering of the symmetry gives rise to a strong enhancement of the MAE.

The aim of the present paper is to investigate the uniaxial MAE of tetragonal and trigonal structures of Fe, Co, and Ni, as well as their linear magnetoelastic coupling coefficients, from first principles. The purpose is to estimate the *bulk* contribution to the MAE of epitaxially grown films and heterostructures. The tetragonal structures considered here are placed along the so-called Bain path that connects the bcc with the fcc structure. A second path of distortion connects the bcc with the fcc structure via trigonal structures, includ-

ing the simple cubic (sc) structure as an intermediate phase. The focus is on the trends of the MAE as a function of the distortion from the cubic symmetry. The calculations employ infinite crystals, thereby neglecting interface and surface effects, as it is often found that for thicker films the MAE is dominated by volume contributions due to epitaxial strains.[12,17] For all the structures studied here a ferromagnetic order is assumed, even though it is not necessarily the ground state in some cases.[18–23] For example, tetragonal structures of Fe close to the fcc structure have been predicted to be antiferromagnetic.[19,21–24] This has been confirmed experimentally in thin Fe films on Cu(001).[2,3] However, it is important to note that the structural stability and the magnetic order of a real magnetic film are crucially dependent on the details of preparation and the interaction of the film with the substrate and/or adjacent layers.

II. COMPUTATIONAL DETAILS

First-principles calculations of the MAE of the ferromagnetic transition metals in their bulk phases are not completely accurate in reproducing the experimental values.[25–27] For bcc Fe and hcp Co the correct easy axes are found, whereas the absolute values of the MAE are less accurate. In the case of Ni the wrong easy axis is obtained, even if the number of approximations involved is reduced to a minimum.[26] The results for bcc Fe are improved when the generalized gradient approximation (GGA) is used instead of the local-density approximation (LDA), but not for hcp Co and fcc Ni.[28]

As was pointed out by Jansen,[29] the failure of the density-functional theory to describe the MAE is the neglect of many-body correlations that—besides the SOC—give rise to orbital moments. A scheme to mimic the effect of the correlations, which in atomic physics is described by Hund's second rule, is the orbital polarization (OP) suggested by Eriksson *et al.*[30] Calculations including both SOC and OP successfully describe the orbital moments of the ferromagnetic transition metals and their alloys.[26,31–33] The inclusion of OP in MAE calculations, however, usually gives values that are too high in comparison with experiment.[17,26] The correct easy axis for fcc Ni was obtained using the LDA+U method, which takes into account the Coulomb and exchange interactions between the d electrons in a mean-field approximation.[34] In these calculations an additional parameter, the so-called Hubbard U, appears and is usually chosen to reproduce experimental results. However, the value of U that reproduced the MAE for fcc Ni was subsequently criticized not to correspond to a realistic number.[35] For structures with a symmetry lower than cubic, e.g., thin films and multilayers, first-principles calculations successfully reproduce, at least, the trends of the MAE.[17,36–40]

All calculations presented here were done with a fully relativistic implementation of the full-potential linear muffin-tin orbital (FP-LMTO) method.[41] The crystal is divided into nonoverlapping muffin-tin spheres centered around the atomic sites and an interstitial region in between. Inside the muffin-tins the density and potential are expanded by means of spherical harmonics times a radial component. In the interstitial region the expansion of the density and potential makes use of a Fourier series. The interstitial basis functions are Bloch sums of Neumann and Hankel functions that are augmented by a numerical basis function inside the muffin-tin spheres, in the standard way of the LMTO method.[42,43]

The scalar-relativistic corrections were included in the calculation of the radial basis functions inside the muffin-tin spheres, whereas the spin-orbit coupling was included at the variational step, as described below.[42] A so-called double basis was used to ensure a well converged wave function, i.e., two interstitial basis functions with different tail energies were used, each attached to its own (n,ℓ) radial function. For the exchange-correlation potential the LDA was chosen for most calculations, as parametrized by von Barth and Hedin. For the determination of the linear magnetoelastic coupling coefficients the GGA (PW91) was used for comparison in some cases. From past experience it is hard to conclude which exchange-correlation potential approximation results in the best MAE. It also seems clear that one should neglect the OP correction, which we have done.

The above explained method was used to calculate the uniaxial MAE, which for tetragonal structures is defined as $\Delta E = E^{100} - E^{001}$, where E^{100} and E^{001} are the total energies with the magnetization in the [100] and [001] directions, i.e., perpendicular or parallel to the c axis, respectively. For trigonal distortions the MAE is defined as $\Delta E = E^{1\bar{1}0} - E^{111}$.

The MAE was evaluated from the force theorem, i.e., as the difference of the eigenvalue sums for the two magnetization directions.[25,44] First, the electron density was calculated self-consistently with a scalar-relativistic Hamiltonian, using the point-group symmetries that are common to both magnetization directions. Then, in a subsequent step, the eigenvalues were obtained by a single diagonalization for each magnetization direction, using the fully relativistic Hamiltonian and the scalar-relativistic self-consistent potential.

For the integration in reciprocal space two different methods were used. Most of the discussion in the remainder focuses on the results that were obtained with the modified tetrahedron method (MTM) by Blöchl *et al.*,[45] using approximately 6×10^4 **k** points in the full Brillouin zone (BZ). The advantage of the MTM is that it is exact in the limit of an infinite number of **k** points. For comparison, the BZ integration was performed with the special points method[46,47] as well, using approximately 3×10^4 **k** points in the full BZ. A Gaussian broadening of 20 mRy was applied to the eigenvalues close to the Fermi energy. The Gaussian broadening method (GBM) has been widely used for MAE calculations recently, but suffers from the fact that the exact result is only recovered in the limit of vanishing smearing, or using higher-order terms in the expansion of the δ function in Hermite polynomials.[48] Correction terms to the GBM and the closely related Fermi-Dirac broadening method have been discussed in Ref. 49. Because of the nonlinear behavior of the MAE in the case of epitaxial strains,[50–57] such as the tetragonal and trigonal structures considered in Secs. III and IV, very small strains were used for the determination of the linear magnetoelastic coupling coefficients in Sec. VI. These calculations were performed with approximately 5×10^5 **k** points in the full BZ. To test the effect of the BZ integration on the magnetoelastic coupling coefficients the eigenvalue sum was cal-

culated with both BZ integration methods mentioned above. All calculations were done at the experimental equilibrium volume of the respective element, $v_{\mathrm{Fe}}=11.78$ Å^3/atom, $v_{\mathrm{Co}}=11.08$ Å^3/atom, and $v_{\mathrm{Ni}}=10.93$ Å^3/atom.

III. UNIAXIAL MAGNETIC ANISOTROPY ENERGY OF TETRAGONAL Fe, Co, AND Ni

If the c axis of the bcc unit cell is elongated to $\sqrt{2}$ times its original length, the crystal transforms to fcc. Likewise, the fcc unit cell can be transformed to bcc by reducing the c axis accordingly. This path of distortion is often referred to as the Bain path. The strain matrix used to describe a volume conserving tetragonal distortion is

$$\begin{pmatrix} \frac{1}{\sqrt{1+\epsilon_z}} & 0 & 0 \\ 0 & \frac{1}{\sqrt{1+\epsilon_z}} & 0 \\ 0 & 0 & 1+\epsilon_z \end{pmatrix}, \tag{1}$$

where the strain along the c axis is related to the c/a ratio by $\epsilon_z=(c/a)^{2/3}-1$.

The calculated uniaxial MAE for tetragonal Fe, Co, and Ni is shown in Fig. 1. For Fe the calculations were done with respect to the bcc structure, i.e., $c/a=1$ corresponds to bcc while $c/a=\sqrt{2}$ is fcc. The calculations for Co and Ni were performed with respect to the fcc structure, i.e., $c/a=1$ is identical to fcc, while $c/a=1/\sqrt{2}$ corresponds to bcc.

The uniaxial MAE increases strongly for all three elements if the cubic symmetry is broken, for reasons that were discussed above. For Co and Ni (middle and lower panel in Fig. 1) the uniaxial MAE is *regular* in the sense that it varies approximately linearly at small distortions from the cubic structures and reaches a maximum in magnitude (at least one maximum is required in order to connect the two symmetry dictated nodes centered at the cubic structures) at tetragonal structures halfway between bcc and fcc. For Co the easy axis is along the [100] direction for c/a ratios between bcc and fcc, while it is perpendicular to it for $c/a<1/\sqrt{2}$ and $c/a>1$. For Ni the situation is reversed, i.e., the easy axis is along the [001] direction for the tetragonal structures between bcc and fcc and along [100] otherwise. The absolute value of the MAE of Co and Ni reaches a maximum of ≈ 250 μeV/atom at $c/a\approx 0.8$–0.85.

The main difference between Co and Ni is the different sign of the uniaxial MAE for the tetragonal structures. This is intimately connected to the different signs of the magnetoelastic coupling coefficients of these two elements (cf. Table I) and can be understood in terms of the difference in band filling, in a rigid-band picture.[61]

The uniaxial MAE for tetragonal structures of Fe (upper panel of Fig. 1) shows a more complicated dependence on the distortion. As for Co and Ni, the MAE varies approximately linearly for small distortions from the cubic structures. On the bcc side, however, the linear region is much smaller. For c/a ratios between bcc and fcc, and small distortions from the cubic symmetry, the easy axis is along [001], while it is along the [100] direction for $c/a<1$ and $c/a>\sqrt{2}$, respectively. Distorting all the way from bcc to fcc, two extra reorientations of the easy axis take place. At $c/a\approx 1.07$ it changes from [001] to [100], and back to [001] at $c/a\approx 1.36$. An analysis of this anomaly is given in Sec. V.

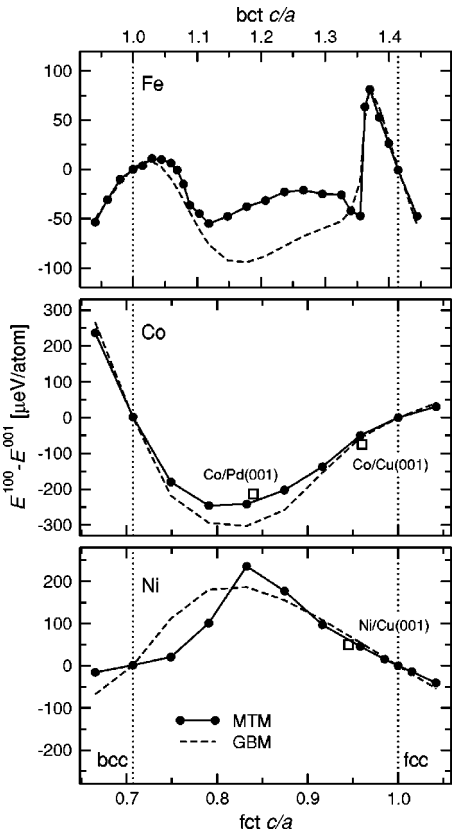

FIG. 1. Calculated uniaxial MAE for tetragonal Fe, Co, and Ni as a function of the c/a ratio using the LDA. MTM and GBM denote the different Brillouin-zone integration techniques used. The vertical dotted lines indicate the bcc (left) and fcc (right) structures. Experimental results are shown as open squares (Refs. 58–60).

Let us now compare the uniaxial MAE obtained from the two different BZ integration methods. For Co the GBM and the MTM yield almost the same results, although the GBM slightly overestimates the MAE. For Ni both methods yield virtually the same MAE for structures close to fcc ($c/a>0.9$). At the bcc end, however, the MAE is strongly overestimated by the GBM. In the case of Fe the results agree qualitatively and quantitatively for distortions close to fcc. At intermediate c/a ratios, in the range between the extra spin reorientations, the GBM overestimates the MAE and gives a qualitatively different behavior. The observed differences in the MAE calculated from the two different BZ integration techniques are not surprising, as the exact value of the MAE is crucially dependent on the detailed topology of the Fermi surface. Since the GBM smears out these details to a certain extent, a false value for the MAE might be obtained. In Gd metal, e.g., the GBM yields a qualitatively wrong behavior of the MAE.[62]

For comparison, experimental results are displayed as open squares in Fig. 1. These values are estimated volume

TABLE I. Calculated and measured linear magnetoelastic coupling coefficients B_1 and B_2 for bcc Fe, fcc Co, and fcc Ni. The theoretical results are from the present work, Wu and Freeman (WF) (Ref. 66), and Komelj and Fähnle (KF) (Refs. 54–57). The results by WF and the experimental values are calculated from magnetostriction coefficients using experimental elastic constants (Refs. 67 and 68). The experimental results for fcc Co are extrapolated from measurements on Co-rich PdCo alloys (Refs. 69 and 70).

	This work		WF		KF		Expt.
	LDA	GGA	LDA	GGA	LDA	GGA	
B_1 (MJ/m^3)							
bcc Fe	−8.3	−4.8	−7.4 (Ref. 66)	−4.1 (Ref. 66)	−10.1 (Ref. 54)	−2.4 (Ref. 54)	−3.3[a]
fcc Co	−13.8	−5.9	−9.0 (Ref. 66)	−5.5 (Ref. 66)	−15.9 (Ref. 56)	−9.8 (Ref. 56)	−12.7[b]/−6.8[c]
fcc Ni	13.9	13.7	8.9 (Ref. 66)	7.9 (Ref. 66)	12.6 (Ref. 55)	10.2 (Ref. 55)	9.2[d]
B_2 (MJ/m^3)							
bcc Fe	−8.9				−7.0 (Ref. 57)	−3.9 (Ref. 57)	10.5[a]
fcc Co	10.6				3.0 (Ref. 57)	4.5 (Ref. 57)	19.3[b]/5.5[c]
fcc Ni	38.8				16.9 (Ref. 57)	11.1 (Ref. 57)	10.2[d]

[a]Bulk, 0 K, Ref. 71.
[b]Bulk, 0 K, Ref. 69.
[c]Film, room temperature, Ref. 70.
[d]Bulk, room temperature, Ref. 71.

contributions to the uniaxial MAE and can therefore be compared to the first-principles results. The excellent agreement between the experimental and the calculated values might be somewhat fortunate, as the precise determination of the epitaxial strains in thin films is not a trivial task. Furthermore, the data for Co/Pd(001) superlattices[58] and thin Co films on Cu(001) (Ref. 59) were obtained at room temperature, whereas the calculations are done for 0 K. The MAE value for thin Ni films on Cu(001) (Ref. 60) was extrapolated to 0 K.

IV. UNIAXIAL MAGNETIC ANISOTROPY ENERGY OF TRIGONAL Fe, Co, AND Ni

The second path of distortion considered here connects the bcc structure and the fcc structure via trigonal structures. A trigonal distortion is described by

$$\begin{pmatrix} d & \epsilon & \epsilon \\ \epsilon & d & \epsilon \\ \epsilon & \epsilon & d \end{pmatrix}, \tag{2}$$

where the diagonal elements d are chosen to conserve the unit-cell volume. The bcc structure corresponds to $\epsilon=0$, while fcc corresponds to $\epsilon=0.5$. Additionally, the sc structure is passed along this path for a distortion of $\epsilon=0.25$.

In Fig. 2 the calculated uniaxial MAE for trigonal structures of Fe, Co, and Ni is shown. The positions of the cubic structures are indicated by vertical dotted lines. In general, the strain dependence of the MAE is more complicated for the trigonal structures than for the tetragonal structures presented in Fig. 1.

In the case of trigonal Fe (upper panel) three reorientations of the easy axis are observed between bcc and fcc, including the symmetry dictated node at the simple cubic structure. The easy axis is along [111] for small strains close to bcc, and reaches a maximum value of ≈ 100 μeV/atom. Around $\epsilon=0.15$ the easy axis flips to the $[1\bar{1}0]$ direction with approximately the same amplitude. Between sc and fcc the behavior is qualitatively similar, but with a slightly reduced maximum MAE.

For trigonal Co (middle panel), the easy axis is along the [111] direction between bcc and sc and reaches a maximum value of ≈ 250 μeV/atom, while it changes to $[1\bar{1}0]$ around sc with a maximum absolute value of ≈ 120 μeV/atom for $\epsilon \approx 0.3$. Around $\epsilon=0.48$ an additional reorientation of the easy axis occurs and the MAE becomes highly nonlinear in the vicinity of fcc (see inset).

For trigonal Ni (lower panel) the situation is complicated by the fact that the magnetic moment almost vanishes close to the bcc structure ($\epsilon<0.1$) and at trigonal strains around 0.4. This is accompanied by a strongly reduced MAE. For strains slightly larger than 0.1 the easy axis points first along [111] and switches then to the $[1\bar{1}0]$ direction, with a maximum value of 320 μeV/atom. Between sc and fcc the easy axis points along [111], with about the same maximum value. Around $\epsilon=0.4$ the MAE is small due to the reduced magnetic moment. For trigonal structures close to bcc, and $\epsilon<0$, the MAE increases strongly. At $\epsilon=-0.05$, e.g., it amounts to 800 μeV/atom, with a magnetic moment of $0.46\mu_B$. The difference in total energy between this trigonally strained bcc structure and the equilibrium fcc structure is only 300 meV. Hence, thin Ni films with a considerably large PMA might be obtained by pseudomorphic growth on a (111) surface, such that the Ni unit cell is close to bcc and contracted along the growth direction. To our knowledge, no experimental results on the MAE of such systems have been published so far.

For the trigonal structures of all three elements both BZ integration techniques (MTM and GBM) yield qualitatively similar results. Experimental results for the MAE of trigonal structure with accurately determined strains are rare. In the most prominent system, Co/Cu(111), the MAE is strongly

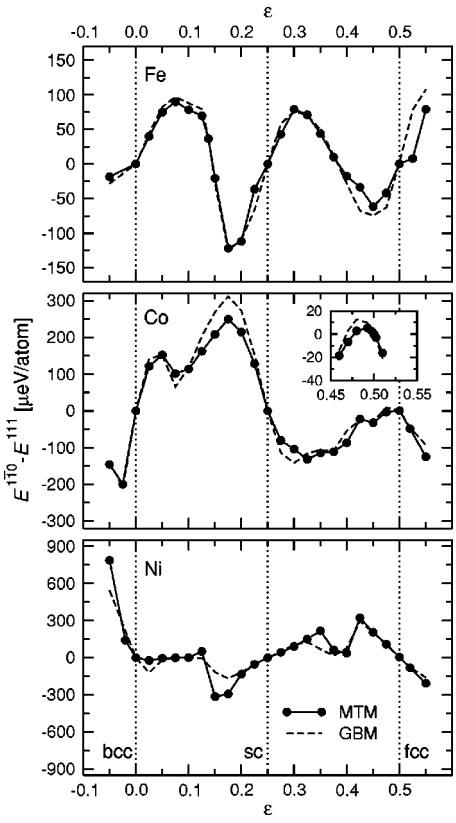

FIG. 2. Calculated uniaxial MAE for trigonal Fe, Co, and Ni as a function of the trigonal strain ϵ using the LDA. MTM and GBM denote the different Brillouin-zone integration techniques used. The vertical dotted lines indicate the bcc (left), sc (middle), and fcc (right) structures. The inset shows the MAE of Co at small distortions from fcc.

dependent on the growth conditions and even changes sign between different experiments.[13,14,63]

V. ANALYSIS OF THE Fe ANOMALY

To explain the anomalous behavior of the MAE in tetragonal Fe (described in Sec. III), a closer look at the electronic structure at the Fermi energy is needed. The Fermi level of Fe is situated in a valley of the density of states, where only a few bands cross E_F. Hence, the influence from one band on the MAE might be very strong, which calls for a band-structure analysis.

In Fig. 3 we show the d dominated eigenvalues of the spin-down band at the high-symmetry Γ point, close to the Fermi level. For bcc Fe $(c/a=1)$ the triply degenerate t_{2g}-like eigenvalues are situated at ≈ -0.38 eV below the Fermi level, and the doubly degenerate e_g-like eigenvalues are situated at ≈ 1.4 eV above the Fermi level. A tetragonal distortion splits these eigenvalues. The t_{2g}-like eigenvalue with the orbital character d_{xy} moves upward in energy while the e_g-like eigenvalue with $d_{x^2-y^2}$ orbital character moves downward. In the fcc limit the $d_{x^2-y^2}$ state becomes a d_{xy} state, and vice versa, due to a 45° rotation of the coordinate system between the two structures. However, on the fcc side, the collapse of the spin moment[64] makes the situation even more complex, and this part is therefore excluded from Fig. 3. If fixed spin moment calculations were used, the curves would be more or less symmetric around a distortion halfway between bcc and fcc. The spin-up d dominated eigenvalues at the Γ point are below the energy range of Fig. 3 and hence all occupied.

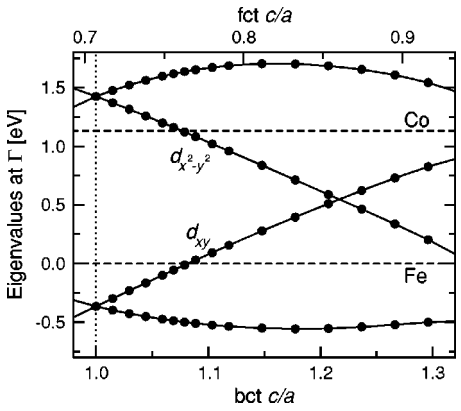

FIG. 3. Calculated d dominated spin-down eigenvalues at the Γ point of tetragonal Fe relative to the Fermi energy as a function of the c/a ratio. The Fermi energies of Fe and Co are indicated by dashed lines. The energy scale is chosen so that E_F is at zero for Fe.

Close to the first reorientation of the easy axis at $c/a \approx 1.07$, the d_{xy} eigenvalue crosses the Fermi level of Fe (lower dashed line in Fig. 3) and becomes unoccupied. From a perturbation treatment of the SOC, it has been found that the major cause of the reorientation of the easy axis is the SOC between the occupied d_{xy} and the unoccupied $d_{x^2-y^2}$ eigenvalues that disappear when the d_{xy} eigenvalue becomes unoccupied.[65] Hence the reorientation of the easy axis for tetragonal Fe (Fig. 1) is consistent with the band crossing shown in Fig. 3.

In order to estimate the influence of the eigenstates at the Γ point on the MAE, a calculation was performed for $c/a = 1.089$ where 2% of the total amount of **k** points, contained in a sphere centered at the Γ point, were excluded from the summation of the eigenvalues. This leads to a shift of the MAE from -36 μeV/atom to $\approx +30$ μeV/atom and, consequently, a reorientation of the easy axis from [100] to [001]. Hence, the anomalous behavior of the uniaxial MAE in tetragonal Fe is connected to a topological change of the Fermi surface occurring at the center of the BZ, which is driven by a structural distortion.

For Co, where no anomaly is seen, the dependence of the eigenvalues on the distortion looks similar to that of Fe. Thus, Fig. 3 applies also for Co if the Fermi level is raised up to ≈ 1.1 eV (upper dashed line) to take into account the correct band filling. The Fermi level of Co, however, is not situated in a valley of the density of states, i.e., there are many bands crossing E_F, that contribute to the MAE. Co is therefore less sensitive to the influence of one band around the Γ point. Finally, for Ni the situation is completely different since the Fermi level is above all the eigenvalues shown in Fig. 3.

VI. MAGNETOELASTIC COUPLING

The linear magnetoelastic coupling coefficients of a cubic system, B_1 and B_2, can be calculated from the strain depen-

dence of the MAE at small tetragonal and trigonal distortions from the cubic structures. They are related to the more widely used magnetostriction coefficients λ_{100} and λ_{111} by

$$B_1 = -\frac{3}{2}\lambda_{100}(C_{11}-C_{12}) \tag{3}$$

and

$$B_2 = -3\lambda_{111}C_{44}, \tag{4}$$

where C_{11}, C_{12}, and C_{44} are elastic constants. λ_{100} and λ_{111} describe the change of length along [100] and [111], respectively, if the sample is brought from a state of zero average magnetization to a state magnetized along that direction.

Because of the nonlinearity of the MAE close to the cubic structures[50–57] it is crucial for the determination of the magnetoelastic coupling coefficients to consider strains that are sufficiently small, so that a linear dependence of the MAE on strain is observed. B_1 and B_2 are then obtained from the slope of the MAE curve with respect to the distortion at $c/a=1$.

The calculated values from the present work are compiled in Table I together with the theoretical results by Wu and Freeman and Komelj and Fähnle—who both used a full-potential linearized augmented plane-wave method—as well as experimental results. As in the previous theoretical studies, there is a large discrepancy between the experimental and theoretical findings. In the case of Fe, e.g., we obtained the wrong sign of B_2, in agreement with the result of Komelj and Fähnle.[57,72] But even the results from the three theoretical studies differ, though not in a systematic way. The latter can probably be attributed to different **k** point convergence and BZ integration methods, as the values of the linear magnetoelastic coupling coefficients for some of the systems studied here depend crucially on the details of the BZ integration. For Fe, e.g., B_1 changes by 30% upon increasing the amount of **k** points in the full BZ from 6×10^4 to 5×10^5, and the difference between the two BZ integration methods amounts to 40%. The results by Komelj and Fähnle[54–57] were obtained with 1.3×10^5 **k** points in the full BZ zone, and both BZ integration techniques were considered. In Ref. 66, however, the details on how the BZ integration was made are missing. As for the choice of the exchange-correlation potential, it is not clear which of the approximations (LDA or GGA) is to be preferred.

VII. SUMMARY

The uniaxial MAE of tetragonal and trigonal Fe, Co, and Ni was calculated from first principles using the FP-LMTO method and the force theorem. The structures considered here are placed along two paths of distortion connecting the bcc and the fcc structure. As is expected from symmetry considerations, the uniaxial MAE increases by orders of magnitude when the cubic symmetry is broken. For tetragonal structures of Co and Ni the symmetry dictated nodes of the MAE at the cubic structures are connected by single maxima situated halfway between the cubic structures along the Bain path. In the case of tetragonal Fe, however, additional reorientations of the easy axis are observed. This anomaly is analyzed in terms of the eigenvalues of tetragonal Fe at the high-symmetry Γ point, and can be attributed to a topological change of the Fermi surface upon distortion.

For the trigonal structures of all three elements studied here, the dependence of the MAE on distortion is more complicated than for the tetragonal structures. It was found that trigonally distorted bcc Ni should exhibit a MAE of 800 μeV/atom for a strain of $\epsilon=-0.05$.

For comparison, the MAE was calculated using two different BZ integration techniques. It was found that the two methods sometimes yield similar results but in order to have a reliable value of the MAE the modified tetrahedron method is to be preferred.

The linear magnetoelastic coupling coefficients were calculated from the MAE at small distortions from the cubic equilibrium structures of the three elements and compared to experimental and previously published theoretical results. The correct sign and order of magnitude is obtained for all systems, except for B_2 of fcc Ni, which is strongly overestimated by our calculations, and B_2 of bcc Fe, for which the wrong sign is calculated.

ACKNOWLEDGMENTS

We thank John M. Wills for supplying the FP-LMTO code and Ruqian Wu, Klaus Baberschke, and Massimiliano Colarieti-Tosti for fruitful discussions. The financial support of the Foundation for Strategic Research (SSF), the Göran Gustafsson Foundation, and the Swedish Research Council (VR) are gratefully acknowledged. Parts of the calculations were performed at the National Supercomputer Centre (NSC) in Linköping, Sweden.

*Electronic address: till.burkert@fysik.uu.se

[1] *Ultrathin Magnetic Structures*, edited by J.A.C. Bland and B. Heinrich (Springer, Berlin, 1994), Vol. 1.
[2] D. Li, M. Freitag, J. Pearson, Z.Q. Qiu, and S.D. Bader, Phys. Rev. Lett. **72**, 3112 (1994).
[3] R.D. Ellerbrock, A. Fuest, A. Schatz, W. Keune, and R.A. Brand, Phys. Rev. Lett. **74**, 3053 (1995).
[4] O. Heckmann, H. Magnan, P. le Fevre, D. Chandesris, and J.J. Rehr, Surf. Sci. **312**, 62 (1994).
[5] K. Heinz, S. Müller, G. Kostka, B. Schulz, and K. Baberschke, Surf. Sci. **364**, 235 (1996).
[6] F.O. Schumann, S.Z. Wu, G.J. Mankey, and R.F. Willis, Phys. Rev. B **56**, 2668 (1997).
[7] J.W.F. Egelhoff, I. Jacob, J.M. Rudd, J.F. Cochran, and B. Heinrich, J. Vac. Sci. Technol. A **8**, 1582 (1990).
[8] Y. Kamada and M. Matsui, J. Phys. Soc. Jpn. **66**, 658 (1997).
[9] G.A. Prinz, Phys. Rev. Lett. **54**, 1051 (1985).
[10] C. Rau, C. Schneider, G. Xing, and K. Jamison, Phys. Rev. Lett. **57**, 3221 (1986).
[11] D. Tian, F. Jona, and P.M. Marcus, Phys. Rev. B **45**, 11 216 (1992).
[12] C.H. Lee, H. He, F.J. Lamelas, W. Vavra, C. Uher, and R. Clarke,

Phys. Rev. B **42**, 1066 (1990).
[13] M. Zheng, J. Shen, J. Barthel, P. Ohresser, C.V. Mohan, and J. Kirschner, J. Phys.: Condens. Matter **12**, 783 (2000).
[14] J. Camarero, J.J. de Miguel, R. Miranda, V. Raposo, and A. Hernando, Phys. Rev. B **64**, 125406 (2001).
[15] P. Bruno, in *Magnetismus von Festkörpern und Grenzflächen*, Lecture Notes (Forschungszentrum Jülich, Jülich, Germany, 1993), Chap. 24.
[16] M. Colarieti-Tosti (private communication).
[17] O. Hjortstam, K. Baberschke, J.M. Wills, B. Johansson, and O. Eriksson, Phys. Rev. B **55**, 15 026 (1997).
[18] V.L. Moruzzi, P.M. Marcus, K. Schwarz, and P. Mohn, Phys. Rev. B **34**, 1784 (1986).
[19] V.L. Moruzzi, P.M. Marcus, and J. Kübler, Phys. Rev. B **39**, 6957 (1989).
[20] P. James, O. Eriksson, B. Johansson, and I.A. Abrikosov, Phys. Rev. B **59**, 419 (1999).
[21] P.M. Marcus, V.L. Moruzzi, and S.-L. Qiu, Phys. Rev. B **60**, 369 (1999).
[22] S.L. Qiu, P.M. Marcus, and H. Ma, J. Appl. Phys. **87**, 5932 (2001).
[23] M. Friák, M. Šob, and V. Vitek, Phys. Rev. B **63**, 052405 (2001).
[24] E. Sjöstedt and L. Nordström, Phys. Rev. B **66**, 014447 (2002).
[25] G.H.O. Daalderop, P.J. Kelly, and M.F.H. Schuurmans, Phys. Rev. B **41**, 11 919 (1990).
[26] J. Trygg, B. Johansson, O. Eriksson, and J.M. Wills, Phys. Rev. Lett. **75**, 2871 (1995).
[27] S.V. Halilov, A.Y. Perlov, P.M. Oppeneer, A.N. Yaresko, and V.N. Antonov, Phys. Rev. B **57**, 9557 (1998).
[28] A.J. Freeman, R. Wu, M. Kima, and V.I. Gavrilenko, J. Magn. Magn. Mater. **203**, 1 (1999).
[29] H.J.F. Jansen, J. Appl. Phys. **67**, 4555 (1990).
[30] O. Eriksson, M.S.S. Brooks, and B. Johansson, Phys. Rev. B **41**, 7311 (1990).
[31] O. Eriksson, B. Johansson, R.C. Albers, A.M. Boring, and M.S.S. Brooks, Phys. Rev. B **42**, 2707 (1990).
[32] Y. Wu, J. Stöhr, B.D. Hermsmeier, M.G. Samant, and D. Weller, Phys. Rev. Lett. **69**, 2307 (1992).
[33] P. Söderlind, O. Eriksson, B. Johansson, R.C. Albers, and A.M. Boring, Phys. Rev. B **45**, 12 911 (1992).
[34] I. Yang, S.Y. Savrasov, and G. Kotliar, Phys. Rev. Lett. **87**, 216405 (2001).
[35] M.D. Stiles, S.V. Halilov, R.A. Hyman, and A. Zangwill, Phys. Rev. B **64**, 104430 (2001).
[36] G.H.O. Daalderop, P.J. Kelly, and M.F.H. Schuurmans, Phys. Rev. B **44**, 12 054 (1991).
[37] R. Wu, C. Li, and A.J. Freeman, J. Magn. Magn. Mater. **99**, 71 (1991).
[38] K. Kyuno, R. Yamamoto, and S. Asano, J. Phys. Soc. Jpn. **61**, 2099 (1992).
[39] G.H.O. Daalderop, P.J. Kelly, and M.F.H. Schuurmans, Phys. Rev. B **50**, 9989 (1994).
[40] P. Ravindran, A. Kjekshus, H. Fjellvåg, P. James, L. Nordström, B. Johansson, and O. Eriksson, Phys. Rev. B **63**, 144409 (2001).
[41] J.M. Wills, O. Eriksson, M. Alouani, and D.L. Price, in *Electronic Structure and Physical Properties of Solids: The Uses of the LMTO Method*, edited by H. Dreyssé, Lecture Notes in Physics (Springer, Berlin, 2000), pp. 148–167.
[42] O.K. Andersen, Phys. Rev. B **12**, 3060 (1975).
[43] H. L. Skriver, *The LMTO Method: Muffin-tin Orbitals and Electronic Structure* (Springer, Berlin, 1984).
[44] M. Weinert, R.E. Watson, and J.W. Davenport, Phys. Rev. B **32**, 2115 (1985).
[45] P.E. Blöchl, O. Jepsen, and O.K. Andersen, Phys. Rev. B **49**, 16 223 (1994).
[46] H.J. Monkhorst and J.D. Pack, Phys. Rev. B **13**, 5188 (1976).
[47] S. Froyen, Phys. Rev. B **39**, 3168 (1989).
[48] M. Methfessel and A.T. Paxton, Phys. Rev. B **40**, 3616 (1989).
[49] O. Grotheer and M. Fähnle, Phys. Rev. B **58**, 13 459 (1998).
[50] R. Koch, M. Weber, K. Thürmer, and K.H. Rieder, J. Magn. Magn. Mater. **159**, L11 (1996).
[51] G. Wedler, J. Walz, A. Greuer, and R. Koch, Phys. Rev. B **60**, R11 313 (1999).
[52] A. Enders, D. Sander, and J. Kirschner, J. Appl. Phys. **85**, 5279 (1999).
[53] R.Q. Wu, L.J. Chen, A. Shick, and A.J. Freeman, J. Magn. Magn. Mater. **177–181**, 1216 (1998).
[54] M. Komelj and M. Fähnle, J. Magn. Magn. Mater. **220**, L8 (2000).
[55] M. Komelj and M. Fähnle, J. Magn. Magn. Mater. **222**, L245 (2000).
[56] M. Komelj and M. Fähnle, J. Magn. Magn. Mater. **224**, L1 (2001).
[57] M. Komelj and M. Fähnle, Phys. Rev. B **65**, 212410 (2002).
[58] B.N. Engel, C.D. England, R.A.V. Leeuwen, M.H. Wiedmann, and C.M. Falco, J. Appl. Phys. **70**, 5873 (1991).
[59] M. Kowalewski, C.M. Schneider, and B. Heinrich, Phys. Rev. B **47**, 8748 (1993).
[60] M. Farle, A.N. Anisimov, W. Platow, P. Poulopoulos, and K. Baberschke, J. Magn. Magn. Mater. **198-199**, 325 (1999).
[61] P. James, O. Eriksson, O. Hjortstam, B. Johansson, and L. Nordström, Appl. Phys. Lett. **76**, 915 (2000).
[62] M. Colarieti-Tosti, S.I. Simak, R. Ahuja, L. Nordström, O. Eriksson, D. Åberg, S. Edvardsson, and M.S.S. Brooks, Phys. Rev. Lett. **91**, 157201 (2003).
[63] M. Farle, W. Platow, E. Kosubek, and K. Baberschke, Surf. Sci. **439**, 146 (1999).
[64] I.A. Abrikosov, O. Eriksson, P. Söderlind, H.L. Skriver, and B. Johansson, Phys. Rev. B **51**, 1058 (1995).
[65] P. James, Ph.D. thesis, Uppsala Universitet, 1999.
[66] R. Wu and A.J. Freeman, J. Magn. Magn. Mater. **200**, 498 (1999).
[67] R. F. S. Hearmon, in *Elastic, Piezoelectric, Pyroelectric, Piezooptic, Electrooptic Constants, and Nonlinear Dielectric Susceptibilities of Crystals*, edited by K.-H. Hellwege and A.M. Hellwege, Landolt-Börnstein, New Series, Group III, Vol. 11 (Springer-Verlag, Berlin, 1979).
[68] J. Gump, H. Xia, M. Chirita, R. Sooryakumar, M.A. Tomaz, and G.R. Harp, J. Appl. Phys. **86**, 6005 (1999).
[69] H. Fujiwara, H. Kadomatsu, and T. Tokunaga, J. Magn. Magn. Mater. **31-34**, 809 (1983).
[70] H. Takahashi, S. Tsunashima, S. Iwata, and S. Uchiyama, Jpn. J. Appl. Phys., Part 2 **32**, L1328 (1993).
[71] M.B. Stearns, in *Magnetic Properties of 3d, 4d, and 5d Elements, Alloys and Compounds*, edited by H.P.J. Wijn, Landolt-Börnstein, New Series, Group III, Vol. 19a (Springer-Verlag Berlin, 1986).
[72] M. Fähnle, M. Komelj, R.Q. Wu, and G.Y. Guo, Phys. Rev. B **65**, 144436 (2002).